Manuscript File Click here to view linked References

IDENTIFYING CHARACTERISTICS OF PIPEJACKING PARAMETERS TO ASSESS GEOLOGICAL CONDITIONS USING OPTIMISATION ALGORITHM-BASED SUPPORT VECTOR MACHINES

Wen-Chieh Cheng[1,2], Xue-Dong Bai[3], Brian B. Sheil[4], Ge Li[3] and Fei Wang[3]

[1]Professor, School of Civil Engineering, Xi'an University of Architecture and Technology, Xi'an 710055, China. Email: w-c.cheng@xauat.edu.cn

[2]Shaanxi Key Laboratory of Geotechnical and Underground Space Engineering (XAUAT), Xi'an 710055, China

[3]PhD student, School of Civil Engineering, Xi'an University of Architecture and Technology, Xi'an 710055, China. Email: baixuedong@xauat.edu.cn (X.-D. Bai); lige@xauat.edu.cn (G. Li); wangfei@xauat.edu.cn (F. Wang)

[4]RAEng Research Fellow, Department of Engineering Science, University of Oxford, U.K. Email: brian.sheil@eng.ox.ac.uk

Initial submission, 28 Feb 2020

2nd Revision submission, 16 Aug 2020

Main text word count: 5227

Tables: 2

Figures: 14

ABSTRACT

Detecting sudden changes in geological conditions (e.g., karst cavern and fault zone) during tunnelling is a complex task. These changes can cause shield machines to jam or even induce geo-hazards such as water ingress and surface subsidence. Tunnelling parameters that relate closely to the surrounding geology have proliferated in recent years and present a substantial opportunity for the application of data-driven artificial intelligent (AI) techniques that can infer patterns from data without reference to known, or labelled, outcomes. This study explores the potential for support vector machines (SVM) to identify changes in soil type during tunnelling towards reducing the possibility of jamming and geo-hazard development. All tunnelling data were pre-processed to convert time series data into feature-based sub-series. A selection of the most popular parameter optimisation algorithms was explored to improve the accuracy of the AI predictions. Their relative merits were evaluated through comparisons with a recent pipejacking case history undertaken in gravel and clayey gravel soils. The results highlight an exciting potential for the use of optimisation algorithm-based SVMs to identify changes in soil conditions during pipejacking.

KEYWORDS: pipejacking; machine learning; optimisation algorithm; soft ground

INTRODUCTION

Pipejacking is a common means of installing utility (e.g., wastewater, natural gas, electricity) pipelines and/or obtaining soil samples for the purpose of geological evaluation (Cui et al. 2015; Ong et al. 2016; Wang et al. 2019a). It is an increasingly popular alternative to open-cut construction, especially in densely populated urban areas, due to the more efficient construction processes and reduced environmental impact (Chen et al. 2015; Tan and Lu 2017; Tan and Wei 2012; Tan et al. 2015; Wang et al. 2018a; Cheng et al. 2020). Identifying the type of soils encountered during tunnel construction not only reduces the potential of geo-hazard (e.g. water ingress and surface subsidence; Fu et al. 2019; Cheng et al. 2019a) but also prevents unplanned downtimes and operation costs (e.g. jamming of shield; Barla et al. 2006). While geo-hazard prevention techniques exist, there remains significant motivation in the industry to sense a variety of complex geological conditions that is likely to confront during tunnel excavation (Shen et al. 2017; Qiu et al. 2018; Wang et al., 2018b; Zhang et al. 2018; Cheng et al. 2019b; Modoni et al. 2019; Wang et al. 2019b).

In pipejacking, tunnelling parameters such as jacking force, cutter wheel torque, flow rate of feedline, pressure in slurry circulating system, and slurry density are highly variable due to their dependence on a number of influencing factors including surrounding geology, lubrication performance, work stoppage and pipe misalignment (Norris and Milligan 1992; Milligan and Marshall 1998; Milligan and Norris 1999; Chapman and Ichioka 1999; Pellet-Beaucour and Kastner 2002; Rahjoo et al. 2012; Reilly and Orr 2012; Choo and Ong 2015; Sheil et al. 2016; Cheng et al. 2017, 2018, 2019c; Ochmański et al. 2018; O'Dwyer et al. 2018; Ren et al. 2018; Phillips et al. 2019; O'Dwyer et al. 2019; Zhang et al. 2019a). For instance, the total jacking loads F_T required to advance a shield machine consists of the face resistance F_0 and the soil-structure frictional resistance F_s. A significant body of research has indicated that effective lubrication can significantly reduce F_s, whereas work stoppages and pipe misalignment can lead to significant and transient increases in F_s. Conversely, jacking into clayey gravel from gravel can cause an increase in F_0 due to increased contact of the shield face and therefore an increase in F_T. Although previous studies performed over the past three decades have greatly enhanced our understanding of the influencing factors and their influence on F_T, the relationship between surrounding geology and tunnelling parameters remains unclear. Systematic research to reveal the surrounding geology-tunnelling parameters relationship is therefore essential (Wu et al. 2019; Wu and Shao 2019). In particular, identifying the response of tunnelling parameters to sudden change of geological condition (e.g., karst cavern and fault zone) is crucial for shield operators to adopt appropriate and timely countermeasures towards preventing geo-hazard from happening.

Traditionally, the manipulation of tunnelling parameters during pipejacking is highly dependent on the shield operator's accumulated site experience, yet the effectiveness of this process determines the safety of tunnel construction and adjacent properties. This may explain the reoccurrence of geo-hazards that is often seen in daily news and social media worldwide and suggest that people may not be adequately aware of the importance of geo-hazard prevention despite the complexity of real-life geological lithologies (Ong and Choo 2011; Mehdizadeh et al. 2017) and soil-structure interaction (Ong et al. 2003; Ong and Choo 2018; Choo and Ong 2020). The proliferation of tunnelling parameters retrieved from modern tunnel shield machines presents substantial opportunity for the application of data-driven artificial intelligent (AI) techniques that can identify patterns in data without reference to known labels (Sheil et al. 2020). This study examines the potential for data-driven AI techniques to identify the type of encountered soils, reducing the possibility of jamming and potential of geo-hazard. A selection of the most popular AI techniques proposed in the literature were considered for this purpose (Zhang et al. 2017, 2019b, 2020). Their relative merits were assessed by comparing AI predictions to monitored data from a recent case history of pipejacking in gravel and clayey gravel soils.

CLASSIFICATION OF EXCAVATED SOILS: AI TECHNIQUES

Overview

Data-driven approaches identify characteristics of the measured system by utilising information retrieved from the measured data, rather than by modelling the system response. However, in most practical problems the measured data (i.e. the outputs) are not labelled. For this reason, 'unsupervised' machine learning algorithms, used to infer patterns in data without reference to known outcomes, is popular. The aim of this study is to develop an improved understanding of existing pipejacking parameters and their relationship with known geological changes during tunnelling, in which case 'supervised' machine learning is the optimal technique. Some popular examples of supervised machine learning algorithms include Multivariate Adaptive Regression Splines (MARS), Random Forest (RF), and Support Vector Machines (SVMs). MARS is a nonparametric statistical method proposed by Friedman (1991) based on a 'divide and conquer' strategy where the training dataset is partitioned into separate piecewise linear segments (splines) of differing gradients (slope). While MARS generates a flexible model that can handle both linear and nonlinear relationships, it is less accurate for sparse data. RF, first proposed by Breiman (2001), is a nonparametric, 'tree-based' method. Each tree learns from its predecessors and updates the residual errors successively. Trees will learn from an updated version of the residuals when they grow next in the sequence. RF

stops growing when the overall Mean Square Error (MSE) is optimal. While RF is a highly flexible technique it is susceptible to overfitting, particularly for small datasets. In light of these limitations, SVM is adopted for this study. The non-parametric nature of SVMs means that model complexity is not influenced by the number of features (inputs) and they are therefore well-conditioned for high-dimensional datasets. Furthermore, the use of kernels allows this technique to capture complex input-output mapping.

Support Vector Machines

SVMs can create a non-linear decision boundary by mapping the data through linear or non-linear kernels to a space with a high dimension (i.e. the 'feature space'). This means that data points which cannot be separated using a straight line in their original input space are 'lifted' to a new feature space where a straight hyperplane can separate the data into different classes. The hyperplane, mapped back to the original input space, therefore forms a non-linear curve. The hyperplane is represented by Eq. 1.

$$\begin{aligned} \boldsymbol{w} \cdot x_i + b \geq 1 \quad if\ y_i = 1 \\ \boldsymbol{w} \cdot x_i + b \geq -1 \quad if\ y_i = -1 \end{aligned} \tag{1}$$

where $\boldsymbol{w}$ is an adaptive weight vector, x is an input vector, y_i is the associated labels, and b is the bias. The hyperplane determines the margin between the classes; all the data points for the class '-1' are on one side, and all the data points for class '1' on the other (see Fig. 1). The distance from the closest point from each class to the hyperplane is equal. Thus, the constructed hyperplane searches for the maximum margin (termed the 'separating power') between classes. To prevent the SVM classifier from over-fitting noisy data (or to create a 'soft margin'), slack variables ξ_i are introduced here, allowing some data points to lie within the margin and the constant C defines the trade-off between the number of misclassification in the training data and margin maximisation. The objective function of the SVM classifier is the following minimisation formulation:

$$\begin{aligned} \text{Minimise} \quad & \frac{1}{2}\left|\left|w\right|\right|^2 + C\sum_{i=1}^{n}\xi_i, \ \ i = 1,2,\dots,n \\ \text{Subject to} \quad & y_i(w^T \cdot x_i + b) \geq 1 - \xi_i \\ & \xi_i \geq 0, \ \ i = 1,2,\dots,n \end{aligned} \tag{2}$$

where C is the nonnegative penalty constant, n is the number of observations and ξ_i is a slack variable. When this minimisation problem is solved using Lagrange multipliers, the decision function (classification rule) for a data point x then becomes:

$$f(x) = \sum_{i=1}^{n} y_i \alpha_i K(x_i, x_j) + b \tag{3}$$

where α_i is a Lagrange multiplier. Every $\alpha_i>0$ is weighed in the decision function and thus 'support' the machine. As SVMs are sparse, there will be relatively few Lagrange multipliers with a non-zero value. Since the outcome of the decision function only relies on the dot-product of the vectors in the feature space, it is not necessary to perform an explicit mapping to that space. Provided a kernel function K generates the same results, it can be used instead. Although the feature space can be of unlimited dimension (leading to a complex hyperplane), this unnecessary complexity is avoided here. Popular selections for the kernel include linear, polynomial and sigmoidal functions; arguably the most common kernel function, the Gaussian Radial Basis Function (RBF), is also used here:

$$K(x_i, x_j) = exp\left(-\frac{\|x_i - x_j\|^2}{2\gamma^2}\right) \quad (4)$$

where γ is a kernel parameter, which is the width of the RBF, and $||x_i - x_j||$ is the dissimilarity measure. In general, the value of γ varies from 0 to 1.

Feature selection

A typical jacking force-distance plot is non-stationary and is unsuitable for direct application of SVMs. In addition, the use of stationary data is desirable to accentuate patterns in the data. To this end, decomposition procedures can be used to disaggregate time series data into (stationary) feature-based sub-series where a weighted moving average dominates data features retained. Decomposition techniques were first developed by Persons (1919) to isolate salient features of a dataset (e.g., trend seasonality and periodic patterns). One of the most popular decomposition techniques is seasonal-trend decomposition using Loess smoothing (STL; Cleveland et al. 1990) which partitions the global series into three additive components as follows:

$$y_t = P_t + T_t + R_t \quad (5)$$

where P_t, T_t and R_t represent the periodic, trend and residual components respectively. Decomposition of the data involves sequential application of a Loess smoother. In this work, no significant periodic component was identified. Four feature variables (namely the trend and residual components of the measured torque and the total jacking load) were considered here for the application of SVMs. The pipejacking data decomposed into trend and residual components (i.e. without the periodic component) also limited false classifications. The weighted moving average of 3 m was adopted here not only to extract both components, but also to eliminate noise towards accentuating data features. In this paper, the current supplied to the cutterwheel is used as a proxy for torque and therefore the residual and trend torque components are plotted in 'Amps'. Since the variation in cutterwheel torque is more distinct for

tunnelling in gravel (sand) than in other soils, its trend and residual components were used to identify 'gravel'. Pellet-Beacour and Kastner (2002) reported that local variations of total jacking load are generally linked to the varying face resistance. While jacking into fine soil governed gravel or sand layer (e.g. clayey gravel), it is possible for the cutting discs to sink into the cutting face, leading to full cutterhead-ground contact and producing variable face resistance. The trend and residual components of the total jacking load were thus used to detect 'clayey gravel'.

IMPLEMENTATION

The Support Vector Machine (SVM) algorithm discussed above was implemented using the Python module *Scikit-learn* (Pedregosa et al. 2011). All data were pre−processed to maximise the efficiency and performance of the learning process and to ensure that the importance of the input dataset is equalised. A 'min−max scaler' was introduced to scale the dataset (Masters 1993), so that all data were laid between our specified range of minimum and maximum. The min-max scaler transforms the features of the input dataset to lie in the interval from 0 to 1. Given a set of input data x_1, x_2,…x_n, the scaled dataset z_1, z_2,…z_n will be:

$$z_i = \frac{x_i - x_{min}}{x_{max} - x_{min}} \tag{6}$$

where *min* and *max* are our specified minimum and maximum values of the range to scale.

Optimisation of SVM parameters

The SVM used herein has two interdependent hyperparameters, namely *C* and γ. Designing an effective classifier requires the SVM parameters to be configured properly in advance. In this study, the SVM parameters were optimised using (a) genetic algorithm (GA), (b) particle swarm optimisation (PSO), and (c) grid search (GS).

Genetic algorithm (GA) is a search algorithm which initially aims to simulate mechanisms of population genetics and natural rules of survival in pursuit of the ideas of adaptation. A typical GA begins with an initial set of random solutions, called a population. Each member within the population is termed a 'chromosome'. New chromosomes ('offspring') are created either by merging two chromosomes (from the current generation) using a crossover operator or by modifying a chromosome by means of a mutation operator. The parents and offspring that are selected based upon their objective values are key components of a new generation. The main steps to optimise the SVM parameters are described as follows (see Fig. 2):

Step 1: Create initial population and convert each member (chromosome) which individually is composed of C and γ from its genotype into phenotype.

Step 2: Train the SVM classifier using the training dataset for each chromosome to calculate the cross-validation accuracy and validate the model with the testing dataset. Evaluate each chromosome using a fitness function once the cross-validation accuracy is achieved.

Step 3: Terminate the process if the termination criteria are satisfied; otherwise repeat the process with the next generation.

Step 4: Search for better solutions using genetic operations, including selection, crossover, and mutation.

Particle swarm optimisation (PSO) was initially developed by Kennedy and Eberhart (1995) to simulate the graceful choreography of birds. In PSO, each solution represents a 'bird' in the flock and is referred to as a 'particle'. A particle is similar to a chromosome in GAs. Unlike GAs, the birds evolve their social behaviour, and accordingly their movement, towards a particular destination. The process therefore physically mimics a flock of birds when they fly. Each bird looks in a specific direction and they identify the bird that is in the best location when communicating together. Accordingly, each bird flies towards the best bird using a velocity that depends on its current position. Each bird then investigates the search space from its new local position. The process repeats until the flock reaches a desired destination. The birds therefore learn not only from their own experience (local search) but also from the experience of others (global search). The main steps of the process are described as follows (see Fig. 3):

Step 1: Consider the parameters C and γ as swarms and initialise a population of particles with random positions and velocities.

Step 2: Evaluate the objective values of particles according to the normalised mean square error (NMSE), as shown in Eq. 7.

$$\mathrm{NMSE} = \frac{1}{n}\sqrt{\sum_{i=1}^{n}(y-\overline{y})^2} \tag{7}$$

where y and $\bar{y}$ represent the measured and simulated values respectively and n is the number of test samples.

Step 3: Each particle learns from their own best position and corresponding objective value; the best initial particle learns from the whole swarm's best position and corresponding objective value.

Step 4: Update the velocity v_i and position p_i of each particle i using Eqs. 8 and 9.

$$v_{ij}(t+1) = \kappa v_{ij}(t) + c_1\gamma_1\left[p_{i,j}(t) - x_{ij}(t)\right] + c_1\gamma_1\left[g_j(t) - x_{ij}(t)\right],\ \ j = 1,2,\dots,d \tag{8}$$

$$x_{ij}(t+1) = x_{ij}(t) + v_{ij}(t+1) \tag{9}$$

where c_1 and c_2 represent the particle's confidence in itself (cognition) and in the swarm (social behaviour) and therefore control the balance between exploration and exploration tendencies; γ_1 and γ_2 are independent random numbers uniformly distributed in the range of 0 to 1; κ is the inertia weight factor; j denotes the dimensionality of the feature space; $p_{i,j}$ and g indicate the best positions experienced so far by the particle i and the whole swarm respectively at time t. Usually c_1 and c_2 are set equal to 2 so that the particles overfly the desired destination approximately half the time. A relatively high value of c_1 will encourage the particles to move towards their local best positions, while higher values of c_2 will lead to faster convergence to the global best position. Fig. 4 illustrates the movement of a particle according to Eqs. 8 and 9.

Step 5: Evaluate the objective values of all particles by comparing their current position and objective value to their own best ones.

Step 6: Select the best particle of the current swarm in accordance with the best objective value.

Step 7: Terminate the process once the termination criteria are satisfied and output the global best position and corresponding objective value; otherwise return to Step 3.

Grid search (GS) is an exhaustive search based upon a defined subset of the hyperparameter space. The hyperparameters are defined via 'lower bound', 'upper bound' and 'number of steps'. The data is first split into k subsets and in most instances the value of k is set to 10. One subset is used as a testing data and evaluated via the remaining k-1 training subsets. Various combinations of hyperparameters are trialled and the one with the best cross-validation accuracy is selected and used to train a GS-SVM model on the whole dataset. The main steps of the process are described as follows (see Fig. 5):

Step 2: Build a grid search space.

Step 3: Train the SVM with selected parameters using a cross-validation approach.

Step 4: Evaluate the performance of the GS-SVM model.

Step 5: Terminate the process once all parameter combinations have been trialled.

Step 6: Obtain the optimised parameters and re-train the GS-SVM model with the optimised parameters.

A classifier was trained using the initial labelled training set, representing 70% of the entire available dataset. There are four outcomes after the analysis, commonly summarised in a 'confusion matrix': (a) true positive (TP), (b) false negatives (FN – system has failed to identify soil type), (c) false positives (FP – system has erroneously identified soil type) and (d) true negatives (TN). For example, 'TP' denotes a geological condition of gravel which has been correctly identified, while 'FN' indicates that the gravel has been erroneously classified. It is noteworthy that in the classification, sand is classed into 'gravel' soil when the associated changes in cutterwheel torque are similar and that similarly silt and clay are classed into 'clayey gravel' soil as their mechanical behaviour is dominated by fines content. Further, 'TN' indicates that a geological condition of clayey gravel has been correctly identified, while 'FP' denotes that the clayey gravel has been erroneously classed. The four outcomes were considered here to evaluate the performance of the three parameter optimisation algorithms using the discovery rate (DR), or true positive rate, and the false alarm rate (FAR), or false negative rate.

$$\mathrm{DR} = \frac{\mathrm{TP}}{\mathrm{TP} + \mathrm{FN}} \quad (\text{for gravel identification}) \tag{10}$$

$$\mathrm{FAR} = \frac{\mathrm{FP}}{\mathrm{TN} + \mathrm{FP}} \quad (\text{for gravel identification}) \tag{11}$$

$$\mathrm{DR} = \frac{\mathrm{TN}}{\mathrm{TN} + \mathrm{FP}} \quad (\text{for clayey gravel identification}) \tag{12}$$

$$\mathrm{FAR} = \frac{\mathrm{FN}}{\mathrm{TP} + \mathrm{FN}} \quad (\text{for clayey gravel identification}) \tag{13}$$

DRIVES C & D: SHULIN, TAIWAN

Project overview

Cheng (2017, 2018, 2019a,c) describe a total of four drives in the soft alluvial deposits of the Shulin district in Taipei County, Taiwan. Two out of the four drives were considered here to assess the selected AI techniques, namely drives C and D. Fig. 6a shows the location of Drives C and D and associated geological boreholes. The length for Drives C and D was 75 m and 102 m respectively. Overburden depth relative to the tunnel crown for Drives C and D were both measured at 10.8 m. The pipejacking was undertaken using a slurry shield machine with a 1.5 m diameter cutterhead. The trailing concrete pipe of 1.44 m in diameter and 1 m in length ensured a 30 mm overcut was created in the annulus area. The self-weight of each

pipe was 12.6 kN. A highly viscous lubricant with Marsh cone viscosity of 38 mins was injected into the overcut annulus, thereby reducing friction resistance to viscous resistance.

Engineering geology

Fig. 6b presents the geological profile as determined from four geological boreholes (BH1 – BH4) installed close to drives C and D. The phreatic surface was located at approximately 4.5 m below ordnance datum (BOD). Fig. 7 shows the soil properties profile as determined from both field and laboratory tests. In addition, Drives C and D were rammed in a ground predominantly composed of gravel and clayey gravel (Fig. 8). Additional information on the project is available in Cheng et al. (2017, 2018, 2019a,c).

RESULTS AND DISCUSSION

Classification results: drives C and D

The three hyperparameter optimisation algorithms were first considered to evaluate their performance for this problem. To assess the feasibility of the optimisation algorithms, the fitness at each generation was traced, as shown in Fig. 9. It can be observed that for gravel identification at drive C (Fig. 9a), the GA achieved an optimal solution immediately whereas for PSO it was achieved within four generations. In contrast, for drive D the GA technique required 19 generations to achieve an optimal solution, whereas PSO required 42. For the identification of clayey gravel at drive C (Fig. 9b), GA required 71 generations to converge to a final solution whereas PSO required 26 and at drive D the optimal solution was achieved immediately for both techniques. In general, the PSO approach achieved faster convergence than GA. Further, the larger variations of fitness value were observed for drive C, indicating that the hyperparameters have greater influence on the predictions for drive C compared to drive D. The wider the parameter range is, the more possibilities GS has of finding the best combination parameter. However, GS is extremely time consuming especially when the number of possible different combinations of variables is rather high. Therefore, a grid search space ranging from 0.001 to 100 which is divided by a multiple of 10 was adopted here to tackle the indicated issue, hence sacrificing the accuracy of prediction. The results of the parameter optimisation are tabulated in Table 1.

The classification results present henceforth correspond to the optimised hyperparameters. We therefore use the more general terminology, ‘SVM classifier’, in the following sections. Further, we only discuss the cases that failed to correctly class the soil i.e. ‘FN’ in the residual-trend torque plot and ‘FP’ in the residual-trend jacking force plot. The results of the SVM classifier applied to the transformed data for drive C are shown in Fig. 10. Fig. 11 provides the

reader with useful context in relation to the mapping of the TP, TN, FP and FN results from the transformed feature space back to the original (raw) parameter space. The SVM classifier provided excellent predictions with three FNs (see Fig. 10a). In this case, the FNs indicate that the gravels were erroneously classed as clayey gravels. Their locations in the original space are at jacked distances of 17 m, 37 m, and 56 m respectively. In contrast, several FPs appear in the predictions presented in Fig. 10b. FPs denote that the clayey gravels were erroneously identified as gravels. They appear at jacked distances of 35-36 m, 41-45 m, 52 m, and 70 m respectively. The results of the SVM classifier applied to the transformed data for drive D are presented in Fig. 12. These data were also mapped back to the original parameter space, as shown in Fig. 13. The SVM classifier also provided good predictions with five FNs (see Fig. 12a). The five FNs correspond to jacked distances of 22-23 m, 62 m, and 75-76 m respectively (in the original parameter space). Further, the SVM classifier provided predictions with two FPs at jacked distances of 40 m and 95 m respectively, indicating that the majority of the clayey gravels were correctly classed (see Fig. 12b).

Discussion

Most of the gravel sections encountered during drive C were successfully identified (Figs. 10a and 11a). The main cause of the three FNs could be due to the occasional presence of sands, reported by Cheng et al. (2017), which reduced T_t closer to the classification boundary. Further, the clayey gravel was not frequently encountered along the tunnel alignment and the definition of the hyperplane of the SVM classifier therefore proved difficult. However, the gravels at jacked distances of 29 m, 48-49 m, and 57-59 m were correctly classed. The datapoints do not exactly correspond to gravels but sands with T_t below 0.33. The reason to explain why the sands can be classed as gravels is that the lack of clayey gravel datapoints led to some difficulty in defining the hyperplane and the SVM classifier defined the noncontinuous boundaries through bypassing the sand datapoints in order to pursue improved predictive performance.

In contrast, nine FPs appear in the predictions in relation to identification of clayey gravel (Figs. 10b and 11b). A clayey gravel can be identified by satisfying two conditions; $T_t > 0.58$ (2052 kN) and $R_t > 0.58$ (-5 kN). Although the FPs at jacked distances of 35-36 m and 41-45 m corresponded to $R_t > 0.58$, their T_t were below 0.58, likely due to the influence of the surrounding gravels. Although the FPs at jacked distances of 52 m and 70 m had values of $T_t > 0.58$, the misclassifications occurred due to $R_t < 0.58$, caused by traversing into the gravel from the clayey gravel. Surprisingly, the predictions were not influenced by pipe deviation being greater than the threshold of 60 mm between jacked distances of 8 m and 21 m.

There are five FNs in the predictions regarding identification of gravel (Figs. 12a and 13a). The five FNs occurred due to their T_t equal to or below 0.33. These datapoints, correspond to sands rather than gravels which reduced T_t to as low as 0.12 and therefore caused these misclassifications. However, it is noteworthy that the sands at jacked distances of 4 m and 37 m were identified as gravels, most likely because of the gravels occurring at jacked distances of 3 m and 36 m. The surrounding gravels raised T_t to 0.54 and 0.39 respectively, significantly above the 0.33 threshold.

Most of the clayey gravels at drive D were correctly classed since FP = 2 (Figs. 12b and 13b). Here, a clayey gravel was identified as $T_t > 0.2$ (1494 kN) and $R_t > 0.58$ (-12.5 kN). The silt at a jacked distance of 40 m, while tunnelling through the clayey gravel, the jacking force reached a plateau, causing a reduction in R_t. The other misclassification at a jacked distance of 95 m is due to $R_t < 0.58$, induced by jacking into the gravel from the clayey gravel, even though the corresponding value of T_t was greater than 0.2.

The discovery rate (DR) in gravels was calculated as 94.1% and 87.5% for drives C and D respectively. This verifies the use of the trend component T_t of the cutterwheel torque to class gravels. The sands at drive C and striking a buried wooden log caused misclassification of gravel; this explains the difference between the hyperplane constructed for drive D (single straight line) compared to drive C (inconsistent two regions), as shown in Figs. 10a and 12a. Some FNs (i.e. jacked distances of 29 m, 48-49 m, and 57-59 m at drive C and 4 m and 37 m at drive D) would have appeared if the SVM classifier did not pursue improved predictive performance by bypassing the datapoints. DR in relation to identification of clayey gravel was 59% and 96.7% for drives C and D respectively, indicating good performance for the identification of clayey gravels. The clayey gravel can be successfully identified by higher T_t and R_t, in accordance with the established hyperplanes. The lower accuracy of prediction at drive C compared to drive D could be due to the higher content of gravel which reduced T_t below the classification threshold.

As discussed, the relative merits of the three hyperparameter optimisation algorithms were evaluated. Here the DRs and FARs determined using the three hyperparameter optimisation algorithms are summarised in Fig. 13 and Table 2. The PSO algorithm outperformed the other two algorithms. Although the PSO algorithm is more prone to becoming ‘trapped’ in local optima, it provided the best balance between exploration and exploitation tendencies. In contrast, the GS algorithm provided the worst performance. The present analyses revealed that while the GS optimization was robust for the identification of optimal hyperparameter combinations, the required computational time was excessive. It is therefore highly reliable but suitable for only low dimensional datasets.

CONCLUSIONS

This paper has examined the potential for the use of AI techniques to identify geological conditions encountered during pipejacking. A selection of the most popular parameter optimisation algorithms was considered to improve the accuracy and efficiency of the AI predictions, namely genetic algorithms, particle swarm optimisation and grid search. Based on the results and discussion, some main conclusions can be drawn as follows:

(a) Decomposition of the data was implemented to transform the cutterwheel torque-jacking distance relationship and the jacking force-jacking distance relationship into feature-based sub-series for direct application of the SVM classifier. The optimal features were found to be the trend and residual components of both the cutterwheel torque and the total jacking force; the trend component dominated the identification of gravel, whereas the trend component T_t and the residual component R_t controlled the identification of clayey gravel. Further, the particle swarm optimisation algorithm provided the best performance due to its best balance between exploration and exploitation tendencies.

(b) Clayey gravels were not encountered frequently during pipejacking at drive C which caused some difficulty in defining the hyperplane. In addition, the surrounding geology could have implications on T_t, leading to false negatives. Some datapoints with low T_t did not cause false negatives because the SVM classifier bypassed them in order to pursue improved predictive performance. Similarly, surrounding geology could also have implications on T_t and R_t producing false positives. Further selection of highly-discriminant features, while classing the silt and/or sand, is deemed necessary to improve the accuracy of prediction.

(c) The performance of the optimisation algorithms was assessed using four performance pressures, namely, TP, FN, FP and TN, using the DR and the FAR indices. The PSO algorithm performed the best amongst the three optimisation algorithms because it provided the best balance between exploration and exploitation tendencies. While the GS sacrificed the accuracy of predictions with a grid of low fineness.

ACKNOWLEDGEMENTS

This study would not have been possible without financial supports from the Special fund for Basic Scientific Research of Central Colleges, Chang'an University, under Grant No.

300102269502. The third author is funded by the Royal Academy of Engineering under the Research Fellowship Scheme.

DECLARATION OF COMPETING INTEREST

The authors declare that they have no known competing financial interests or personal relationships that could have appeared to influence the work reported in this paper.

AUTHOR CONTRIBUTION

This paper represents a result of collaborative teamwork. Dr. Wen-Chieh Cheng and Dr. Brian B. Sheil prepared the original manuscript and provided edits to the revised manuscript. Mr. Xue-Dong Bai performed a series of analyses and prepared the revised manuscript under the first author's supervision. Mr. Fei Wang, and Miss Ge Li revised the figures and tables and gave edits to the revised manuscript.

REFERENCES

Breiman, L., 2001. Random forests. *Machine Learning*, 45(1), 5-32.

Barla, M., Camusso, M. and Aiassa, S., 2006. Analysis of jacking forces during microtunnelling in limestone. *Tunnelling and Underground Space Technology*, 21(6), 668-683.

Cleveland, R., Cleveland, W., McRae, J., Terpenning, I., 1990. STL: a seasonal-trend decomposition procedure based on loess. *Journal of Official Statistics*, 6, 3-73.

Chapman, D.N. and Ichioka, Y., 1999. Prediction of jacking forces for microtunnelling operations. *Tunnelling and Underground Space Technology*, 14, 31-41.

Chen, R.P., Li, Z.C., Chen, Y.M., Ou, C.Y., Hu, Q., Rao, M., 2015. Failure investigation at a collapsed deep excavation in very sensitive organic soft clay. *Journal of Performance of Constructed Facilities*, 29(3), 04014078.

Cheng, W.C., Ni, J.C., Shen, J.S.L. and Huang, H.W., 2017. Investigation into factors affecting jacking force: a case study. *Proceedings of the Institution of Civil Engineers-Geotechnical Engineering*, 170(4), 322-334.

Cheng, W.C., Ni, J.C., Arulrajah, A. and Huang, H.W., 2018. A simple approach for characterising tunnel bore conditions based upon pipe-jacking data. *Tunnelling and Underground Space Technology*, 71: 494-504.

Cheng, W.C., Ni, J.C., Huang, H.W., Shen, J.S., 2019a. The use of tunnelling parameters and spoil characteristics to assess soil types: a case study from alluvial deposits at a pipejacking project site. *Bulletin of Engineering Geology and the Environment*, 78(4), 2933-2942.

Cheng, W.C., Xue, Z.F., Wang, L., Xu, J., 2019b. Using post-harvest waste to improve shearing behaviour of loess and its validation by multiscale direct shear tests. *Applied Sciences*, 9(23), 5206.

Cheng, W.C., Wang, L., Xue, Z.F., Ni, J.C., Rahman, M., Arulrajah, A., 2019c. Lubrication performance of pipejacking in soft alluvial deposits. *Tunnelling and Underground Space Technology*, 91, 102991.

Cheng, W.C., Li, G., Liu, N., Xu, J., Horpibulsuk, S., 2020. Recent massive incidents for subway construction in soft alluvial deposits of Taiwan: a review. *Tunnelling and Underground Space Technology*, 96, 103178.

Choo, C.S. and Ong, D.E.L., 2015. Evaluation of pipe-jacking forces based on direct shear testing of reconstituted tunneling rock spoils. *Journal of Geotechnical and Geoenvironmental Engineering*, 141(10), 04015044.

472 Choo, C.S. and Ong, D.E.L., 2020. Assessment of non-linear rock strength parameters for
473 the estimation of pipe-jacking forces. Part 2. Numerical modelling. *Engineering*
474 *Geology*, 265, 105405.
475 Cui, Q.L., Xu, Y.S., Shen, S.L., Yin, Z.Y., Horpibulsuk, S., 2015. Field performance of
476 concrete pipes during jacking in cemented sandy silt. *Tunnelling and Underground*
477 *Space Technology*, 49, 336-344.
478 Friedman, J.H., 1991. Multivariate adaptive regression splines. *The Annals of Statistics*, 19,
479 1-67.
480 Fu, J.Y., Xie, J.W., Wang, S.Y., Yang, J.S., Yang, F., Pu, H., 2019. Cracking performance of
481 an operational tunnel lining due to local construction defects. *International Journal of*
482 *Geomechanics*, 19(4), 04019019.
483 Masters, T. 1993. *Practical neural network recipes in C++*. Academic Press, San Diego, CA.
484 Milligan, G.W.E. and Marshall, M.A., 1998. The functions and effects of lubrication in pipe
485 jacking. *Tunnels and Metropolises, Negro Jr. and Ferreira (eds.), Balkema,*
486 *Rotterdam*, 2, 739-744.
487 Milligan, G.W.E. and Norris, P., 1999. Pipe–soil interaction during pipe jacking. *Proceedings*
488 *of the Institution of Civil Engineers-Geotechnical Engineering*, 137(1), 27-44.
489 Mehdizadeh, A., Disfani, M., Evans, R., Arulrajah, A., Ong, D.E.L., 2017. "Mechanical
490 Consequences of Suffusion on Undrained Behaviour of a Gap-Graded Cohesionless
491 Soil - An Experimental Approach," *Geotechnical Testing Journal*, 40(6), 1026-1042.
492 Modoni, G., Wanik, L., Mascolo Maria, C., Salvatore, E., Bzówka, J., Shen, S.L., Daniele, V.,
493 Pingue, L., 2019. Strength of sandy and clayey soils cemented with single and
494 double fluid jet grouting. *Soils and Foundations*, 59(4), 942-954.
495 Norris, P. and Milligan, G.W.E., 1992. Frictional resistance of jacked concrete pipes at full
496 scale. In *Proceedings of International Conference on Trenchless Construction, No-*
497 *Dig,* 92,121-128.
498 Ong, D.E.L., Leung, C.F., Chow, Y.K., 2003. Piles subject to excavation-induced soil
499 movement in clay. In *Proc. 13th European Conference on Soil Mechanics and*
500 *Geotechnical Engineering, Prague, Czech Republic, vol.2, pp 777-782*.
501 Ong, D.E.L., Choo, C.S., 2011. Sustainable construction of a bored pile foundation system in
502 erratic phyllite. In *ASEAN Australian Engineering Congress 2011, Kuching, Sarawak,*
503 *Malaysia, pp 30-45*.
504 Ochmański, M., Modoni, G., Bzówka, J., 2018. Automated numerical modelling for the
505 control of EPB technology. *Tunnelling and Underground Space Technology*, 75, 117-
506 128.
507 Ong, D.E.L. and Choo, C.S., 2016. Back-analysis and finite element modeling of jacking
508 forces in weathered rocks. *Tunnelling and Underground Space Technology*, 51, 1-10.

O'Dwyer, K.G., McCabe, B.A., Sheil, B.B. and Hernon, D.P. 2018. Blackpool South Strategy project: analysis of pipe-jacking records. *Proceedings of Civil Engineering Research in Ireland (CERI 2018)*.

Ong, D.E.L. and Choo, C.S., 2018. Assessment of non-linear rock strength parameters for the estimation of pipe-jacking forces. Part 1. Direct shear testing and backanalysis. *Engineering Geology*, 244, 159-172.

O'Dwyer, K.G., McCabe, B.A., Sheil, B.B. 2019. Interpretation of pipe-jacking and lubrication records for drives in silty soil. *Underground Space*. DOI: 10.1016/j.undsp.2019.04.001

Persons, W.M. 1919. *Indices of Business Conditions: An Index of General Business Conditions*. Harvard University Press.

Pedregosa, F., Varoquaux, G., Gramfort, A., Michel, V., Thirion, B., Grisel, O., Blondel, M., Prettenhofer, P., Weiss, R., Dubourg, V. and Vanderplas, J., 2011. Scikit-learn: Machine learning in Python. *Journal of machine learning research*, 12(Oct), pp.2825-2830.

Pellet-Beaucour, A.L. and Kastner, R., 2002. Experimental and analytical study of friction forces during microtunneling operations. *Tunnelling and Underground Space Technology*, 17(1), 83-97.

Phillips, B.M., Royston, R., Sheil, B.B. and Byrne, B.W. (2019) Instrumentation and monitoring of a concrete jacking pipe. In *Proceedings of the International Conference for Smart Infrastructure and Construction, Cambridge, UK (Editors De Jong, Schooling, Viggiani), ICE Publishing, pp 457-462*.

Qiu, J.L., Liu, H.Q., Lai, J.X., Lai, H.P., Chen, J.X., Wang, K., 2018. Investigating the long-term settlement of a tunnel built over improved loessial foundation soil using jet grouting technique. *Journal of Performance of Constructed Facilities*, 32(5), 04018066.

Rahjoo, S., Najafi, M., Williammee, R. and Khankarli, G., 2012. Comparison of jacking load models for trenchless pipe jacking. In *Pipelines 2012: Innovations in Design, Construction, Operations, and Maintenance, Doing More with Less*, 1507-1520.

Reilly, C.C. and Orr, T.L., 2012. Analysis of interface friction effects on microtunnel jacking forces in coarse-grained soils. In *Proceedings of the Bridge and Concrete Research in Ireland Conference*, 121-126.

Ren, D.J., Shen, S.L., Arulrajah, A., Cheng, W.C., 2018. Prediction model of TBM disc cutter wear during tunnelling in heterogeneous ground. *Rock Mechanics and Rock Engineering*, 51(11), 3599-3611.

Sheil, B.B., Curran, B.G. and McCabe, B.A., 2016. Experiences of utility microtunnelling in Irish limestone, mudstone and sandstone rock. *Tunnelling and Underground Space Technology*, 51, 326-337.

Sheil, B.B., S.K. Suryasentana, and W.C. Cheng. 2020. An assessment of anomaly detection methods applied to microtunnelling. *Journal of Geotechnical and Geoenvironmental Engineering*, 146(9), 04020094.

Shen, S.L., Wang, Z.F., Cheng, W.C., 2017. Estimation of lateral displacement induced by jet grouting in clayey soils. *Geotechnique*, 67(7), 1-10.

Tan, Y., Lu, Y., 2017. Forensic diagnosis of a leaking accident during excavation. *Journal of Performance of Constructed Facilities*, 31(5), 04017061.

Tan, Y., Wei, B., 2012. Performance of an overexcavated metro station and facilities nearby. *Journal of Performance of Constructed Facilities*, 26(3), 241-254.

Tan, Y., Wei, B., Zhou, X., Diao, Y., 2015. Lessons learned from construction of shanghai metro stations: importance of quick excavation, prompt propping, timely casting and segmented construction. *Journal of Performance of Constructed Facilities*, 29(4), 04014096.

Wang, Z.F., Cheng, W.C., Wang, Y.Q., 2018a. Investigation into geohazards during urbanization process of Xi'an, China. *Natural Hazards*, 92(3), 1937-1953.

Wang, Z.F., Shen, J.S., Cheng, W.C., 2018b. Simple method to predict ground displacements caused by installing horizontal jet-grouting columns. *Mathematical Problems in Engineering*, 2018, 1897394.

Wang, Z.C., Hu, Z., Lai, J.X., Wang, H., Wang, K., Zan, W.B., 2019a. Settlement characteristics of jacked box tunnelling underneath a highway embankment. *Journal of Performance of Constructed Facilities*, 33(2), 04019005.

Wang, Z.F., Shen, S.L., Modoni, G., 2019b. Enhancing discharge of spoil to mitigate disturbance induced by horizontal jet grouting in clayey soil: theoretical model and application. *Computers and Geotechnics*, 111, 222-228.

Wu, K., Shao, Z.S., Qin, S., 2019. Mechanical analysis of tunnels supported by yieldable steel ribs in rheological rocks. *Geomechanics and Engineering*, 19(1), 61-70.

Wu, K., Shao, Z.S., 2019. Study on the effect of flexible layer on support structures of tunnel excavated in viscoelastic rocks. *Journal of Engineering Mechanics*, 145(10), 04019077.

Zhang, W.G., Zhang, Y.M., Goh, A.T.C., 2017. Multivariate adaptive regression splines for inverse analysis of soil and wall properties in braced excavation. *Tunnelling and Underground Space Technology*, 64, 24-33.

579 Zhang, C., Yang, J.S., Ou, X.F., Fu, J.Y., Xie, Y.P., Liang, X., 2018. Clay dosage and
580 water/cement ratio of clay-cement grout for optimal engineering performance. *Applied*
581 *Clay Science*, 163, 312-318.
582 Zhang, P., Chen, R.P., Wu, H.N., 2019a. Real-time analysis and regulation of EPB shield
583 steering using random forest. *Automation in Construction*, 106, 102860.
584 Zhang, W.G., Zhang, R., Wu, C., Goh, A.T.C., Lacasse, S., Liu, Z., Liu, H., 2019b. State-of-
585 the-art review of soft computing applications in underground excavations.
586 *Geoscience Frontiers*, doi: 10.1016/j.gsf.2019.12.003.
587 Zhang, W.G., Li, H.R., Wu, C.Z., Li, Y.Q., Liu, Z.Q., Liu, H.L., 2020. Soft computing
588 approach for prediction of surface settlement induced by earth pressure balance
589 shield tunneling. *Underground Space*, doi: 10.1016/j.undsp.2019.12.003.
590

591 List of figures

Fig. 12 Performance of the PSO-SVM model applied to drive D mapped to transformed parameter space: (a) identification of gravel (C=10.071, γ=0.421) and (b) identification of clayey gravel (C=20.212, γ=13.965)

Fig. 13 Performance of the PSO-SVM model applied to drive D remapped back to initial parameter space: (a) identification of gravel (C=10.071, γ=0.421) and (b) identification of clayey gravel (C=20.212, γ=13.965)

Fig. 14 Performance of the three optimisation algorithms: (a) discovery rate (DR) and (b) false alarm rate (FAR)

592

593 List of tables

594

595

Figure 1

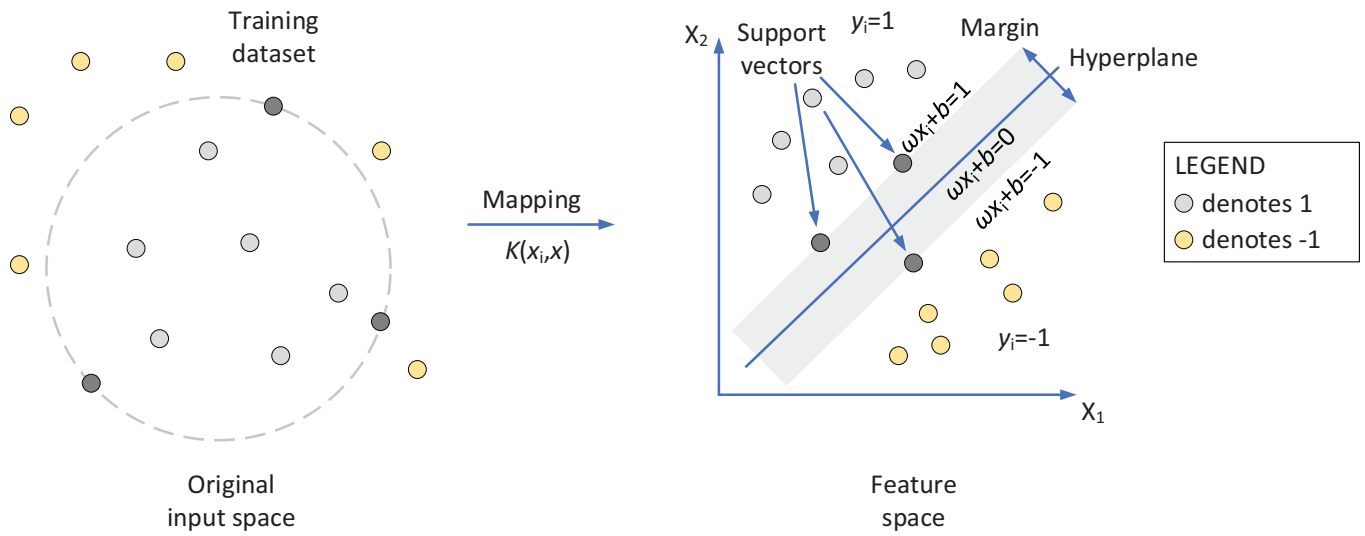

Fig. 1 Illustration of transformation of original input space into feature space for hyperplane determination

Figure 2

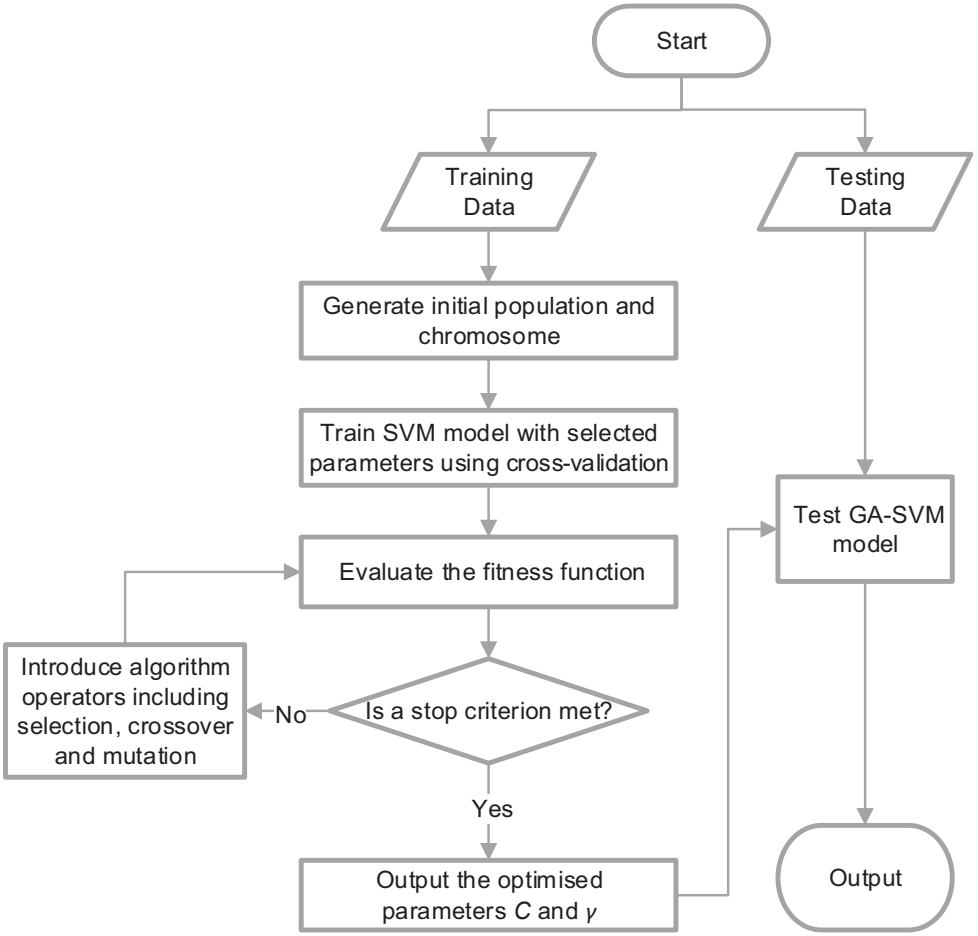

Fig. 2 Flowchart of the GA-SVM algorithm

Figure 3

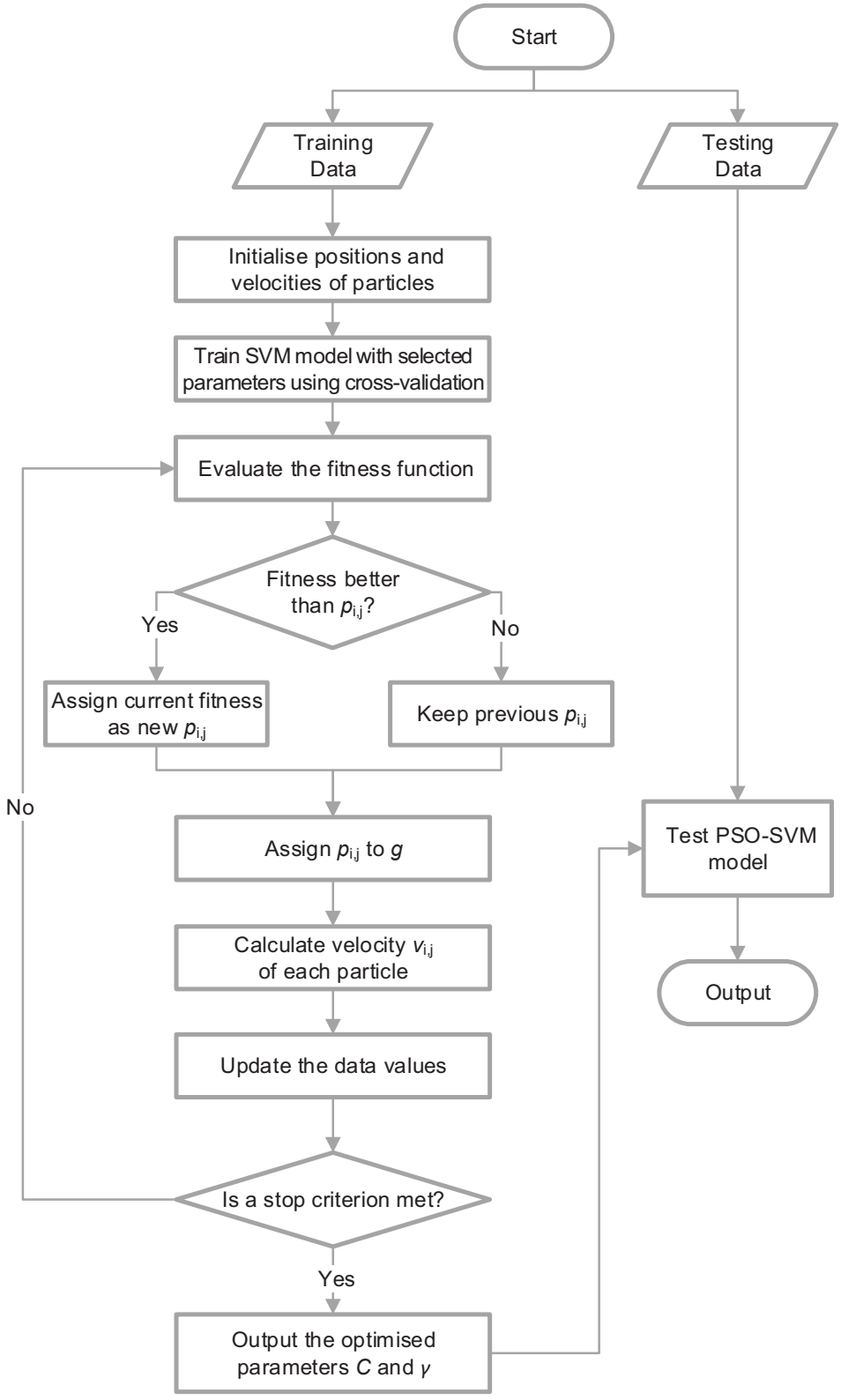

Fig. 3 Flowchart of the PSO-SVM algorithm

Figure 4

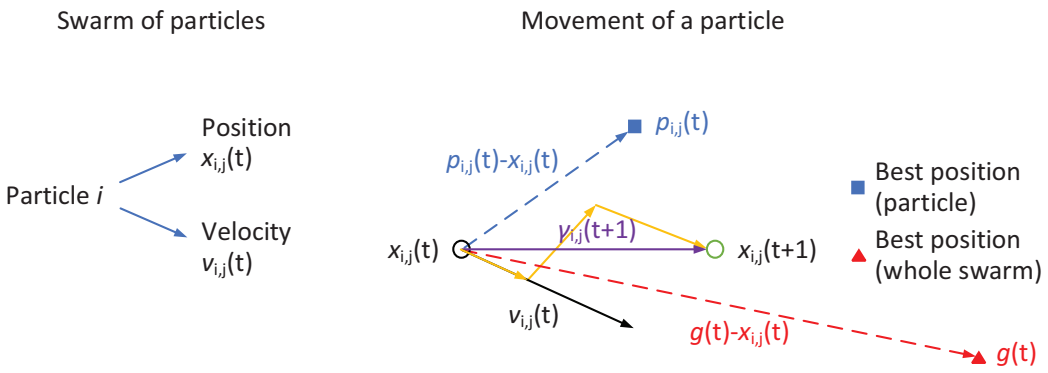

Fig. 4 Illustration of movement of a particle based upon Eqs. 8 and 9

Figure 5

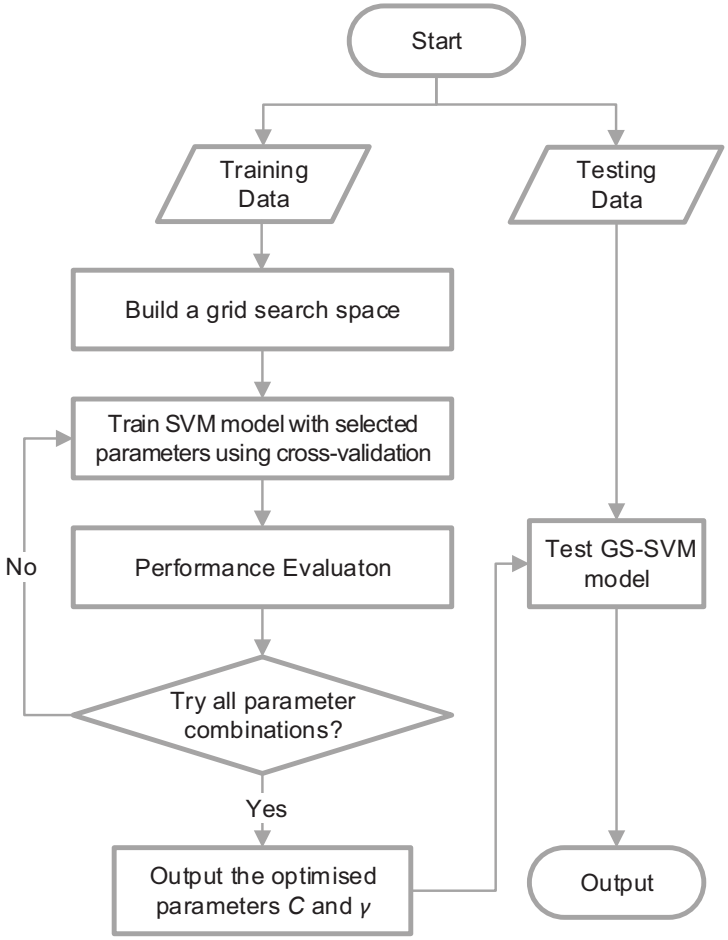

Fig. 5 Flowchart of the GS-SVM algorithm

Figure 6

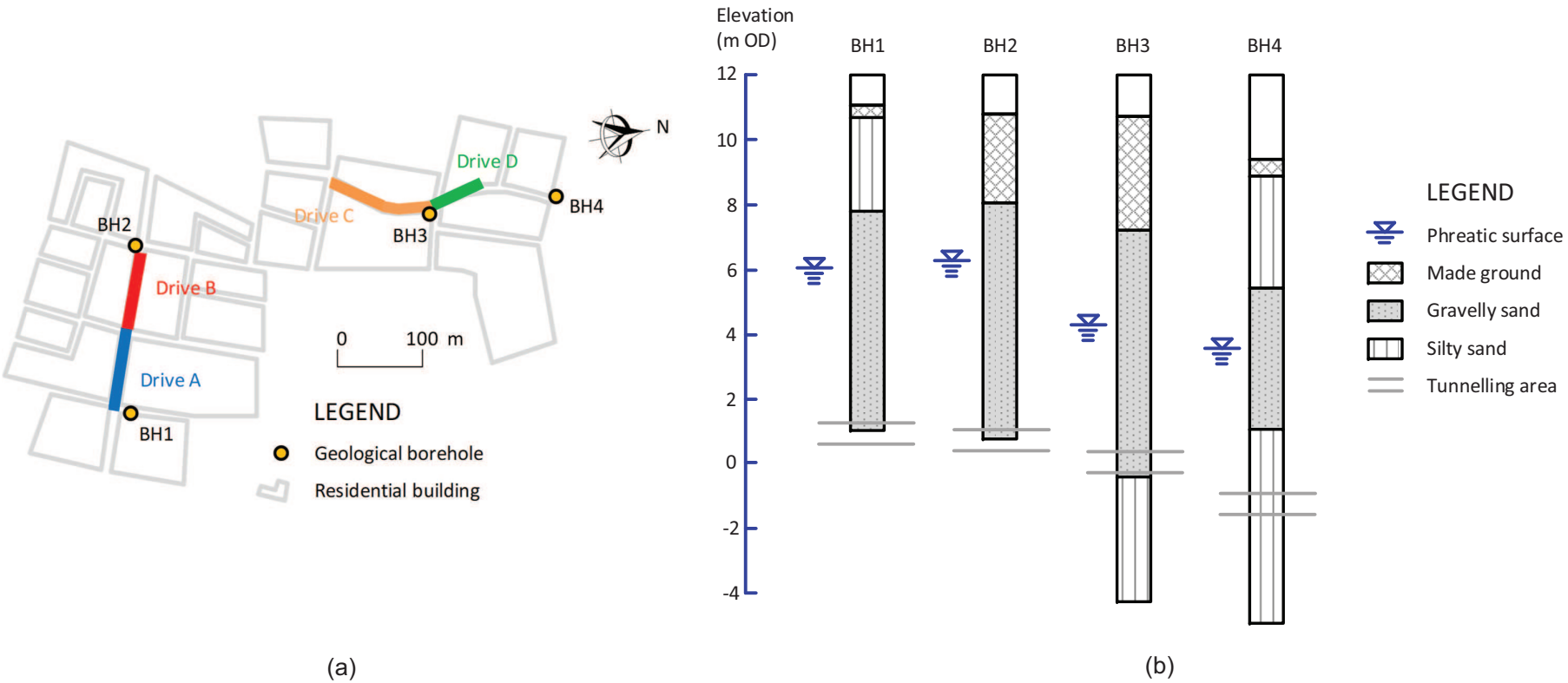

Fig. 6 Project description: (a) location of pipejacking drives and nearby geological boreholes and (b) geological profile along the tunnel alignment

Figure 7

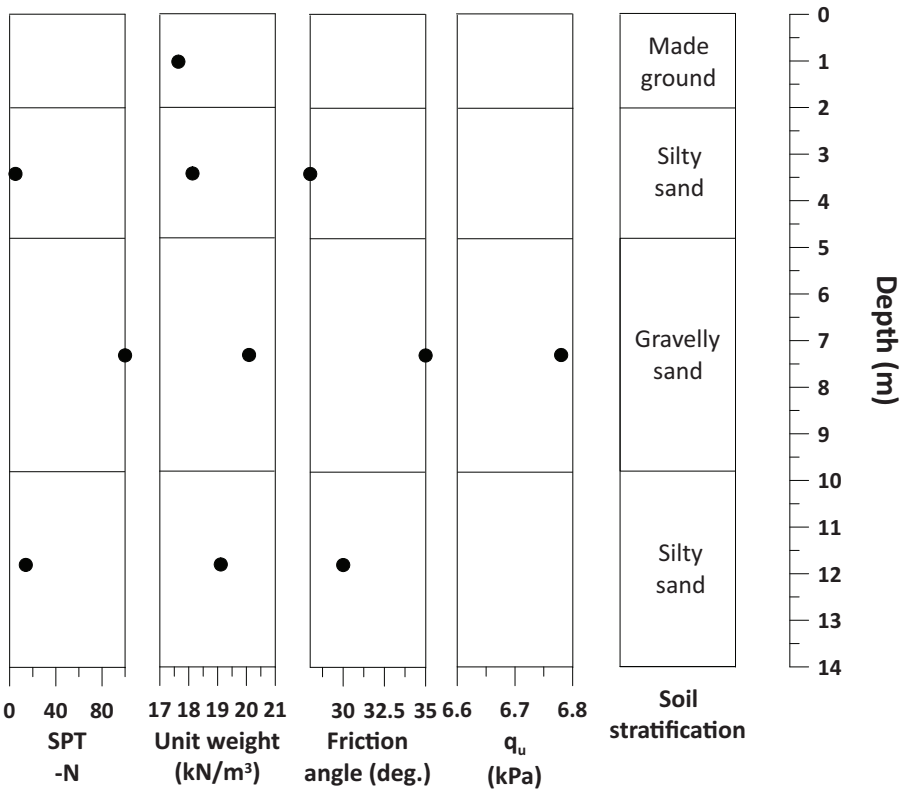

Note: q_u=Unconfined compressive strength; SPT-N=Blow count N value

Fig. 7 Soil properties profile

Figure 8

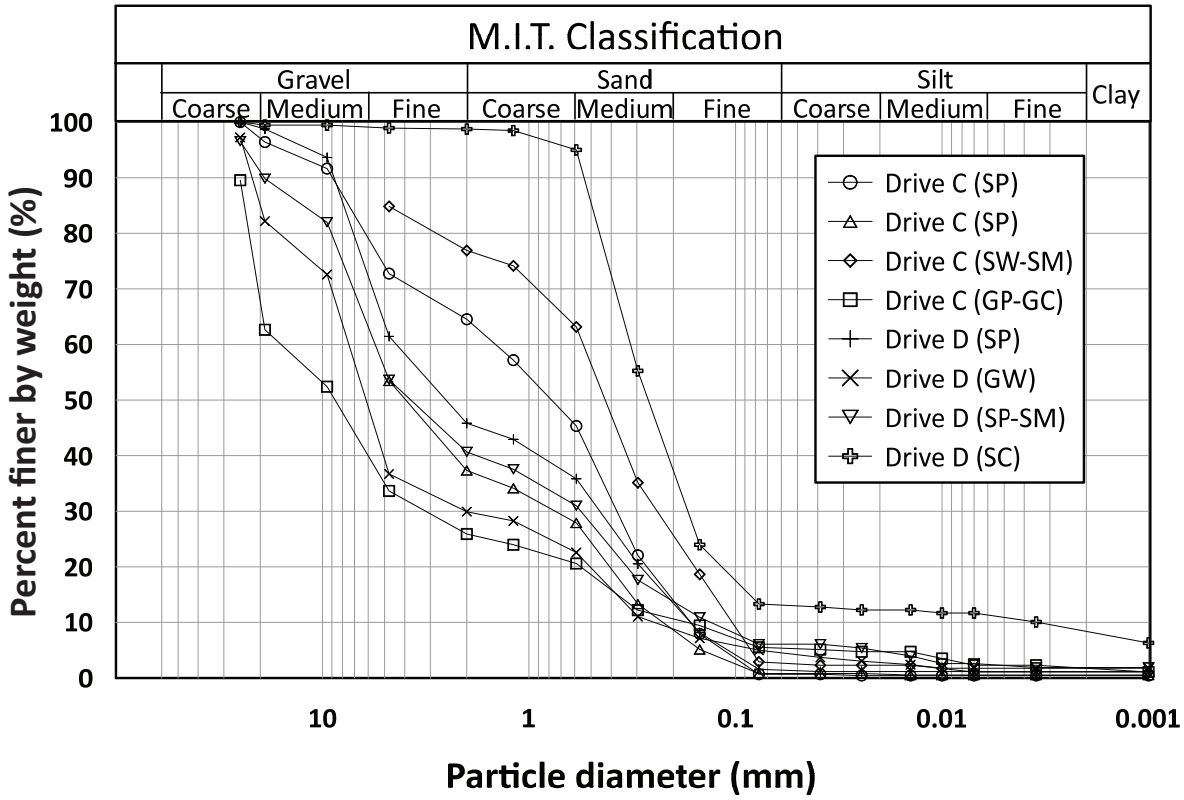

Fig. 8 Grain-size distribution curves for drives C and D

Figure 9

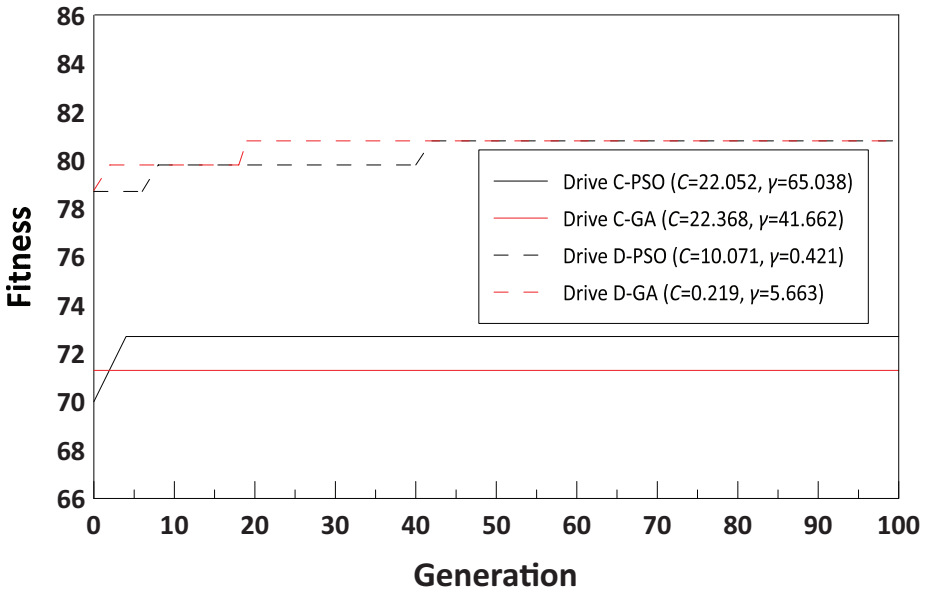

(a)

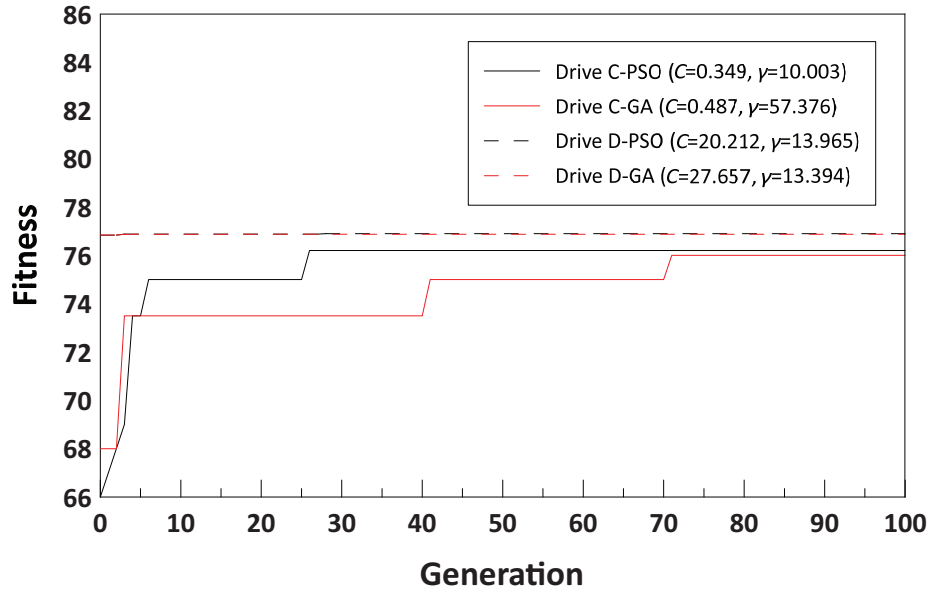

(b)

Fig. 9 Optimised results of the PSO and GA algorithms: (a) gravel identification and (b) clayey gravel identification

Figure 10

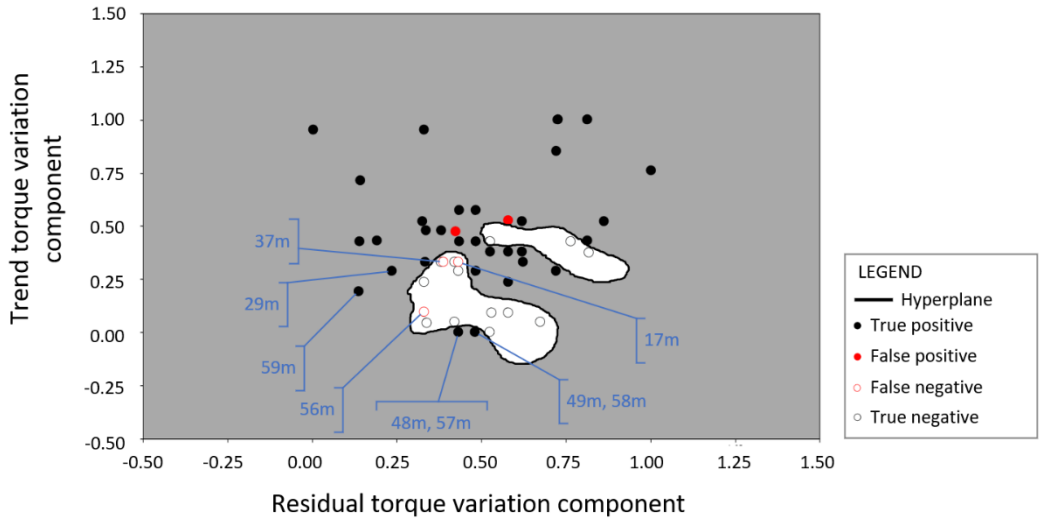

(a)

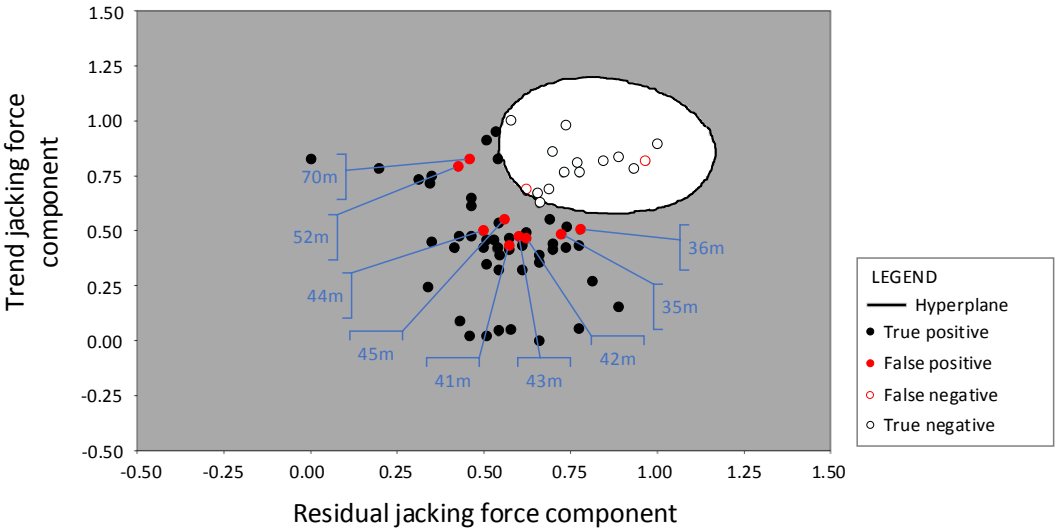

(b)

Fig. 10 Performance of the PSO-SVM model applied to drive C mapped to transformed parameter space: (a) identification of gravel (C=22.052, γ=65.038) and (b) identification of clayey gravel (C=0.349, γ=10.003)

Figure 11

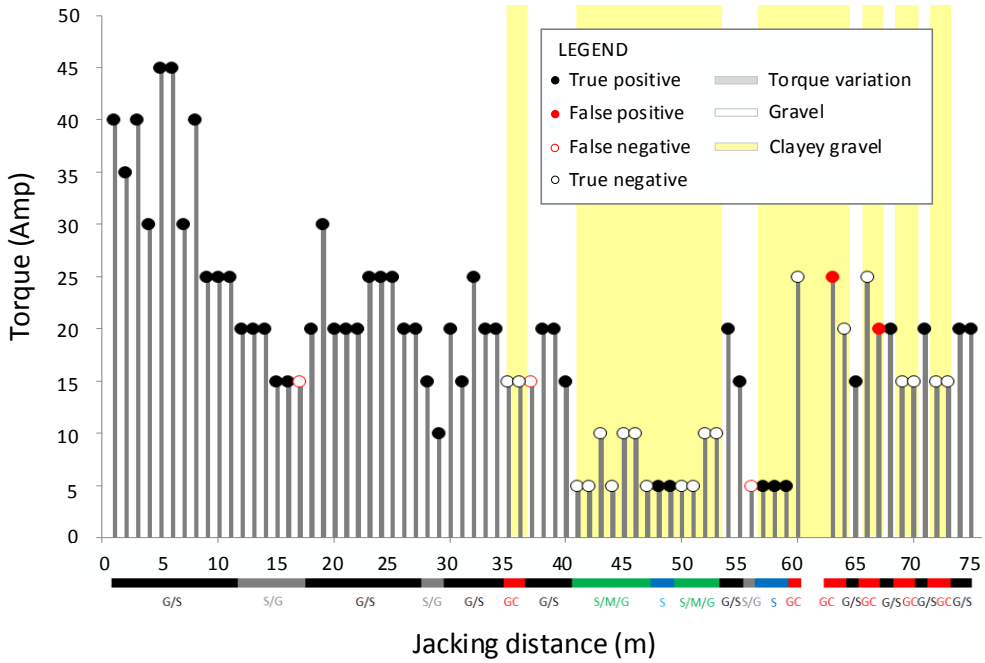

(a)

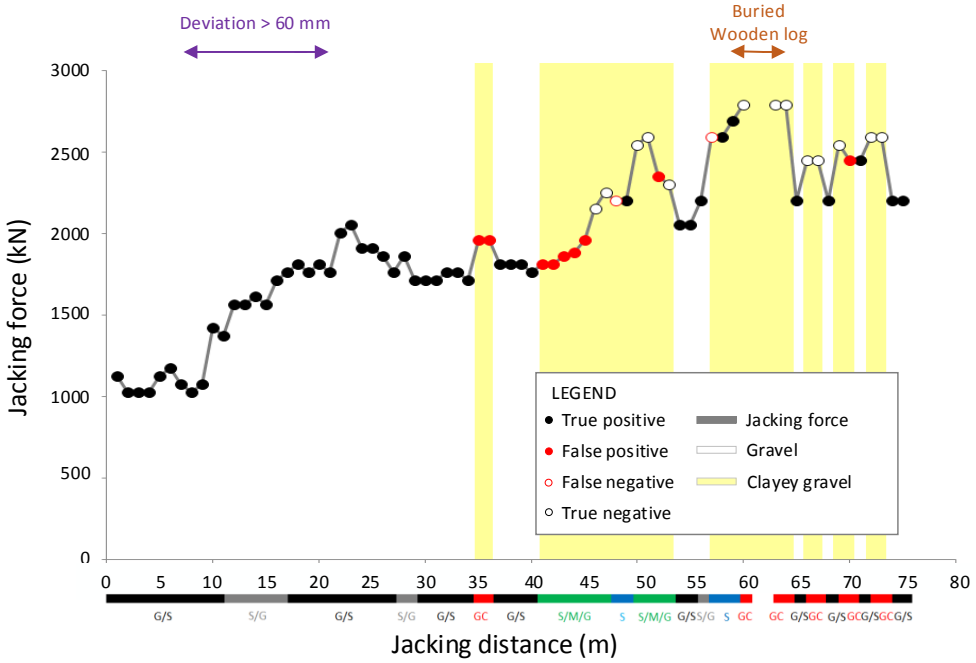

(b)

Fig. 11 Performance of the PSO-SVM model applied to drive C remapped back to initial parameter space: (a) identification of gravel (C=22.052, γ=65.038) and (b) identification of clayey gravel (C=0.349, γ=10.003)

Figure 12

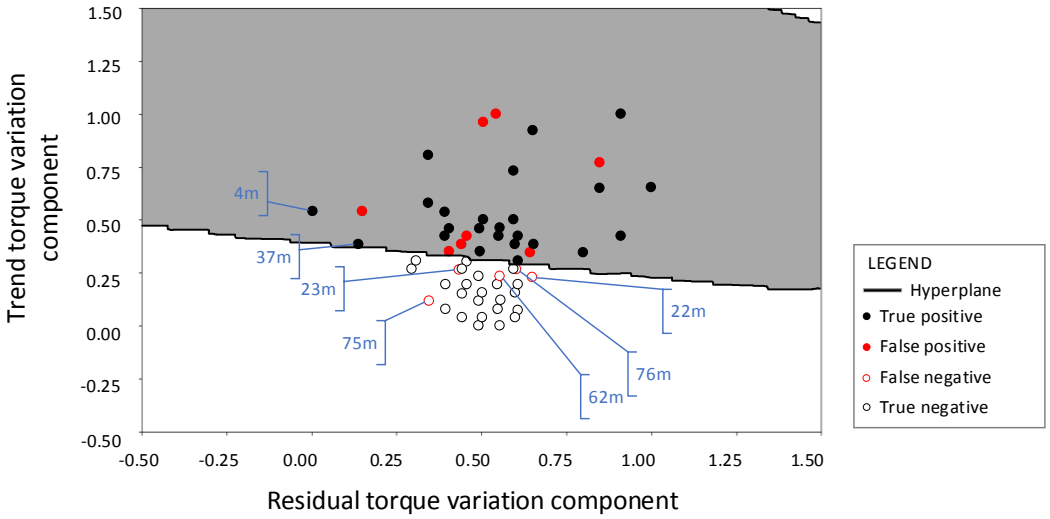

(a)

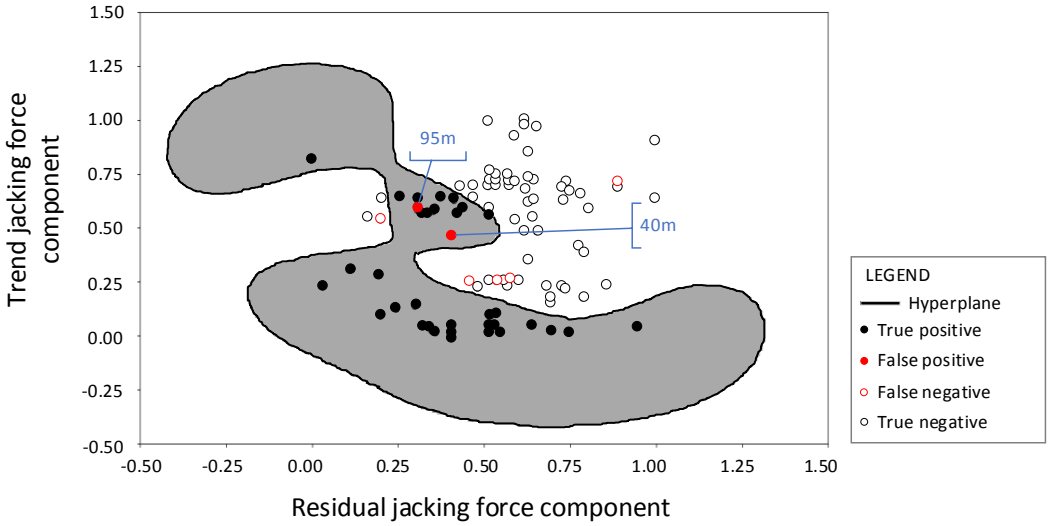

(b)

Fig. 12 Performance of the PSO-SVM model applied to drive D mapped to transformed parameter space: (a) identification of gravel (C=10.071, γ=0.421) and (b) identification of clayey gravel (C=20.212, γ=13.965)

Figure 13

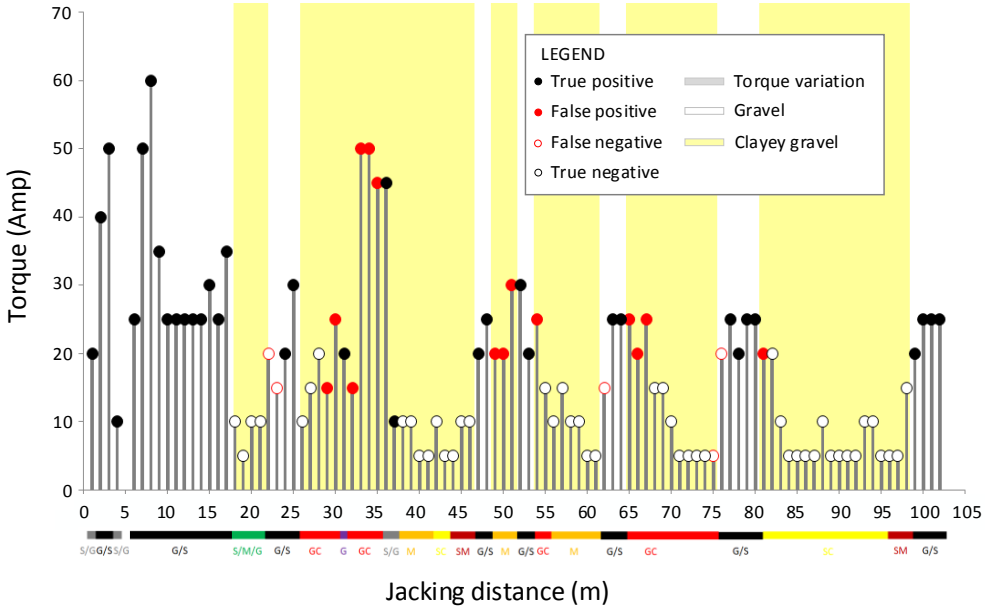

(a)

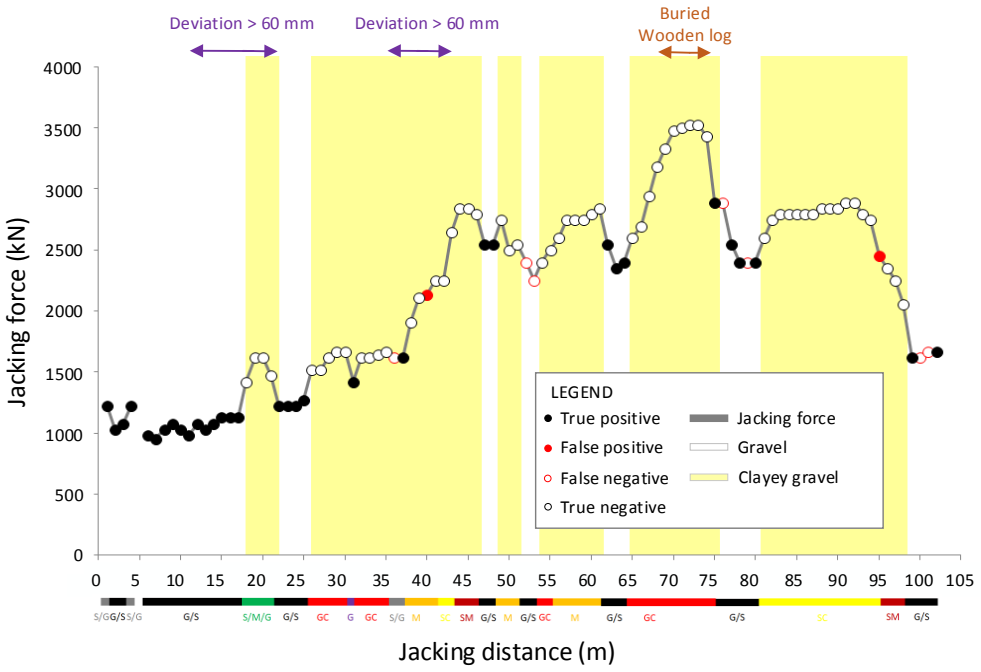

(b)

Fig. 13 Performance of the PSO-SVM model applied to drive D remapped back to initial parameter space: (a) identification of gravel (C=10.071, γ=0.421) and (b) identification of clayey gravel (C=20.212, γ=13.965)

Figure 14

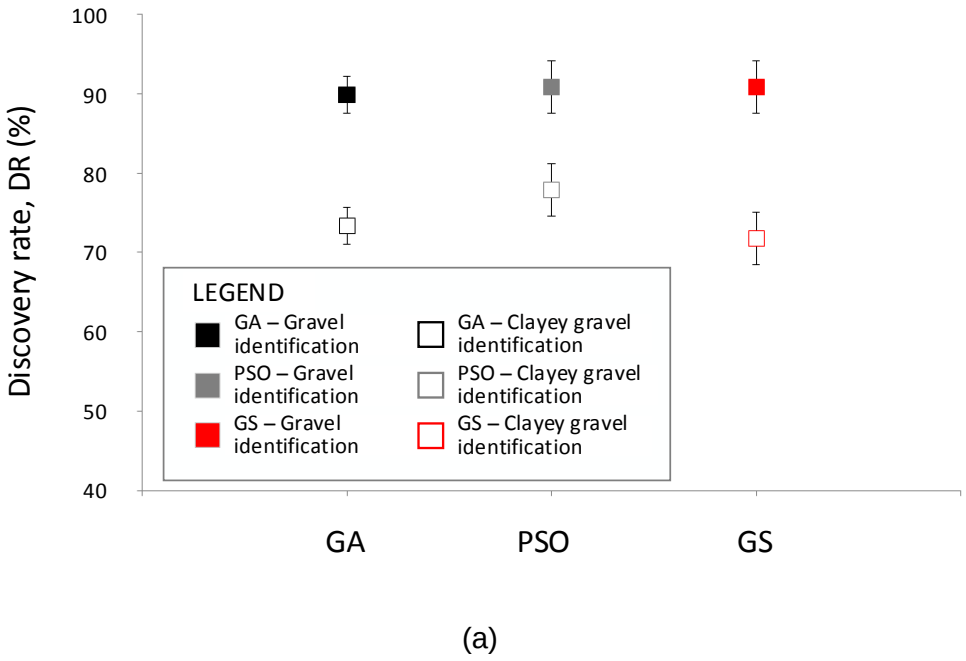

(a)

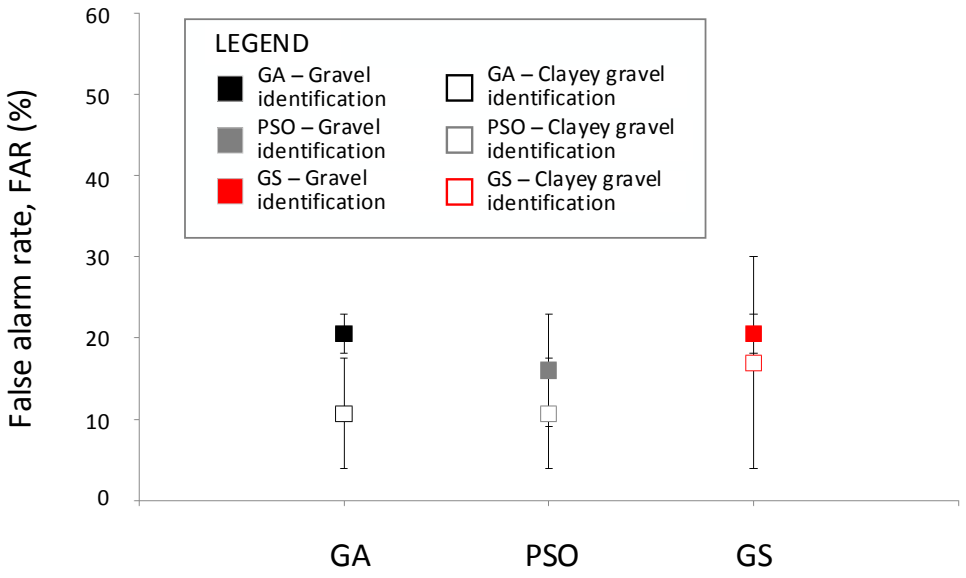

(b)

Fig. 14 Performance of the three optimisation algorithms: (a) discovery rate (DR) and (b) false alarm rate (FAR)

Table 1 Results of the parameter optimisation: (a) gravel identification and (b) clayey gravel identification

(a)

Hyperparameter used in identifying gravel at drive C	Genetic algorithm (GA)	Particle swarm optimisation (PSO)	Grid search (GS)
C	22.368	22.052	100
γ	41.662	65.038	100
Hyperparameter used in identifying gravel at drive D	Genetic algorithm (GA)	Particle swarm optimisation (PSO)	Grid search (GS)
C	0.219	10.071	1
γ	5.663	0.421	1

(b)

Hyperparameter used in identifying clayey gravel at drive C	Genetic algorithm (GA)	Particle swarm optimisation (PSO)	Grid search (GS)
C	0.487	0.349	1
γ	57.376	10.003	1
Hyperparameter used in identifying clayey gravel at drive D	Genetic algorithm (GA)	Particle swarm optimisation (PSO)	Grid search (GS)
C	27.657	20.212	10
γ	13.394	13.965	0.1

Table 2 Performance of the optimisation algorithms: (a) gravel identification and (b) clayey gravel identification

(a)

Drive	Gravel identification					
	DR (%)			FAR (%)		
	GS	GA	PSO	GS	GA	PSO
Drive C	94.1	92.2	94.1	9.1	18.2	9.1
Drive D	87.5	87.5	87.5	22.9	22.9	22.9

(b)

Drive	Clayey gravel identification					
	DR (%)			FAR (%)		
	GS	GA	PSO	GS	GA	PSO
Drive C	50.0	50.0	59.0	7.8	3.9	3.9
Drive D	93.4	96.7	96.7	30.0	17.5	17.5

Note: DR=discovery rate, FAR=false alarm rate, STDEV=standard deviation.